PREDICTION OF WIND LOADS ON A HIGH-SPEED CATAMARAN DURING MANOEUVRING AT LOW SPEED

Reference NO. IJME 782, DOI: 10.5750/ijme.v164iA2.782

S Amani, A D Henderson, J J McVicar, J R Binns, University of Tasmania, Australia

KEY DATES: Submitted: 15/09/21; Final acceptance: 05/10/22; Published: 30/11/22

SUMMARY

The influence of wind on a ship's manoeuvring performance has always been an important issue, particularly in a harbour environment and during the ship's docking or disembarking. Catamarans have a relatively shallow draught and small cross-sectional area below the waterline making station keeping a challenge due to wind loading. It is therefore important that the designer has appropriate tools for accurate station keeping prediction. This paper presents aerodynamic coefficient estimates for a 112 m high-speed wave piercing catamaran built by Incat Tasmania using RANS-based CFD and wind tunnel testing. It demonstrates that CFD and wind tunnel testing can be used to complement each other in quantifying the magnitude and effects of wind loading on a high-speed wave piercing catamaran. The results from the CFD simulations are validated by wind tunnel experiments. The uncertainty in the CFD calculated force coefficients is estimated to be less than 5.8%.

NOMENCLATURE

B	beam (m)
C_D	drift resistance coefficient
CFD	computational fluid dynamics
C_N	yaw moment coefficient
C_X	longitudinal force coefficient
C_Y	lateral force coefficient
EFD	Experimental Fluid Dynamics
Fx	longitudinal force component parallel to the lateral area of the ship (N)
Fy	lateral force component perpendicular to the lateral area of the ship (N)
H	height (m)
IMO	International Maritime Organisation
LOA	overall length of the ship (m)
m	Mass (kg)
M_Z	moment around z axis (N/m)
N	yaw moment (N/m)
P	Pressure (Pa)
$RANS$	Reynolds-averaged Navier–Stokes
R_n	Reynolds number
SF	frontal projected wind area of the ship (m²)
SL	lateral projected wind area of the ship (m²)
U_w	wind velocity (m/s)
y^+	non-dimensional wall distance
∇	displacement volume (m³)
k	turbulent kinetic energy (m²/s²)
ε	turbulent dissipation rate (1/s)
ρ_a	air density (kg/m³)
ρ_w	water density (kg/m³)
ω	turbulent dissipation rate (1/s)
Θ	Wind angle from the bow (degrees)

1. INTRODUCTION

The influence of wind on a ship's manoeuvring performance has always been an important issue, particularly in a harbour environment and during the ship's docking or disembarking. The effect of wind forces is even more noticeable on high-speed catamarans as they are in general much lighter than conventional ships of a similar size. Catamaran, in general, have a large sectional area above the waterline compared with their below waterline area due to relatively shallow draught. The shallow draught gives large catamarans the advantage of being able to travel in places where the water depth is only a few metres. If improperly designed, shallow draught vessels can experience difficulties with course keeping in rough seas, particularly when they face strong winds or currents. This also applies when they are travelling at low speeds, predominantly when they are manoeuvring for berthing. Special care must be taken by the designer if such vessels are required to remain stationary for a period of time in rough seas, such as during the transfer of a ship's crew to or from offshore platforms. Published literature provides little guidance on proper analysis methods for high-speed wave-piercing catamarans. The current market demands that catamaran ships become larger in size and travel faster with increased fuel efficiency. These ships must carry larger loads and operate in places where they are constantly facing strong winds and currents. The behaviour of these ships in such conditions affects the safety of the passengers, crew, cargo and the ship itself. The importance of having accurate knowledge of the wind loads on ships for improved station keeping, fuel efficiency, comfort and safety of the passengers has been discussed in a number of studies (Aage *et al.,* 1997; Oura & Ikeda, 2007; Sadovnikov, 2009; Andersen, 2012; Janssen *et al.*, 2017; Majidian & Azarsina, 2018; Formela, 2018).

It may be argued that catamarans have superior station keeping compared with monohulls due to a larger distance between their waterjets which are located in two separate hulls. The use of waterjets enables thrust to be vectored in different directions on demand, whereas for vessels

Figure 1. 112m catamaran built by Incat Tasmania (Luttrell 2017)

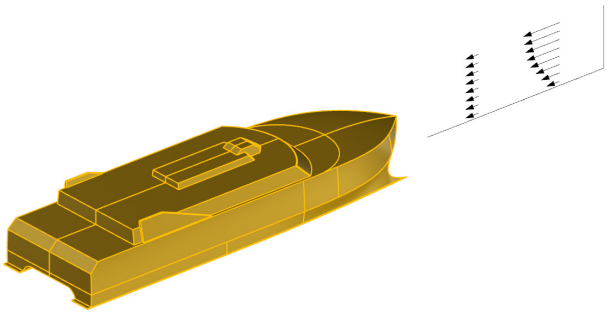

Figure 2. Combined local wind field caused by a ship's movement and the natural wind velocity profile over the ocean surface

with rudders, a flow across the rudder is required to generate a side component of thrust, and the effectiveness differs in forward and reverse thrust. Nevertheless, even catamarans with waterjets may not have sufficient station keeping in high wind conditions, especially in harbour environments when they travel at low speed (Sadovnikov, 2009). Sadovnikov claims that for high-speed craft there is increased risk of losing control over the vessel because they are normally operated on short routes, with several departures and approaches per day at low speed. Travelling at low speed for berthing or disembarking when a strong wind is present may cause collisions with other vessels or marine structures.

Calculation of the wind forces on full scale ships is very difficult and expensive. There is very little published full-scale data from aerodynamic forces on ships. Generally, the prediction of aerodynamic forces for the purpose of studying station keeping is determined by using either analytical methods (Fujiwara *et al.*,1998; Sadovnikov, 2009; Formela ,2018) or experimental methods (Oura & Ikeda ,2007; Tasumi and Ikeda, 1999; Andersen, 2012; Janssen *et al.*, 2017).

The limitations in experimental testing can be predominantly attributed to several factors: uncertainty in the wind profile, proper constraint and control of the heading, and similarity issues when extrapolating results to full scale (Amani, 2019). Computational Fluid Dynamics methods have been developed to a stage in which they offer a realistic computational alternative to the experimental methods (Aage *et al.,* 1997; Tu *et al.,* 2013). However, it is well known that verification and validation studies are required to establish confidence in accuracy of the CFD simulations (Wnęk *et al.* 2010). Once a CFD model is validated, it can be used as an alternative to experimental testing of scale models, which may include testing in towing tanks and wind tunnels.

1.1 ATMOSPHERIC BOUNDARY LAYER

A ship moving on a smooth sea and in still air experiences a resistance component arising from the movement through the air of the part of the hull which is above the water. This resistance depends on the speed of the ship, the projected area and shape of the upper structure and the relative direction of the wind (Larsson & Raven, 2010). The relative wind field experienced by the ship is the superposition of the local wind field and the ship's motion. (Larsson & Raven, 2010; Andersen, 2012). This is shown in Figure 2.

It is well known that correctly reproducing the atmospheric boundary layer profile is essential for accurate modelling (Polsky, 2002; Forrest & Owen, 2010; Andersen, 2012; Janssen *et al.,* 2017; Vogt *et al.,* 2017). The boundary layer within the wind tunnel should therefore closely approximate the same characteristics found in a full-scale atmospheric boundary layer. The relationship between the mean velocity U_z and height above the surface z, for a boundary-layer of height δ and a mean velocity of U_∞ at height δ, can be described by the power law:

$$\frac{U_z}{U_\infty} = \left(\frac{Z}{\delta}\right)^{\alpha} \quad (1)$$

The power law exponent α defines the shape of the boundary layer velocity profile. Generally, the value of α depends on the roughness of the terrain and over the open ocean can be taken as $\alpha \approx 0.11$ (Hsu *et al.,* 1994; Lubitz & White, 2004). Reproducing the relative wind field inside a wind tunnel is challenging. However, as the primary interest of this study is to assess the control envelope at low-speed, the local wind field is of much larger magnitude than the relative wind field resulting from the vessel's motion.

2. WIND TUNNEL TESTING

Experimental testing was performed in a closed-loop octagonal-section wind tunnel at the University of Tasmania as shown in Figure 3. A 1:300 scale model of a Incat Tasmania 112 m wave piercing catamaran was used in this study. The model size was selected according to the size of the test section available for wind tunnel testing. The 1:300 scale model has the total height of 59 mm which is measured from the top of the ship's bridge to the waterline. Table 1 shows the principal particulars of both full scale 112 m ship and the scale model.

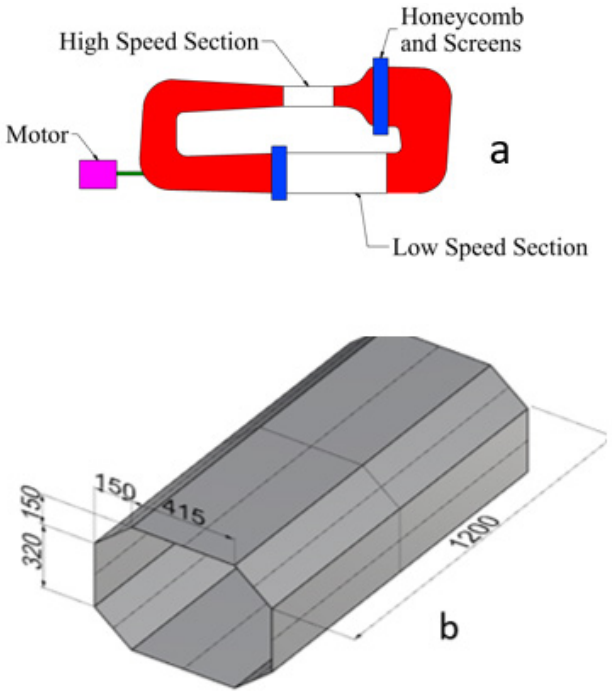

Figure 3. a) The closed-loop wind tunnel and b) Isometric view of the high speed section (dimensions in mm).

Table 1: Details of the Incat Tasmania 112m wave piercing catamaran and scale model.

	Full scale	Model scale
Gross tonnage	8000 ton	–
LOA	112.6 m	–
Length of demi hull	105.6 m	0.352 m
Breadth	30.5 m	0.101 m
Draught	3.7 m	
Speed	40 knots (20.57m/s)	14.25 m/s

Oura & Ikeda, (2007) performed experimental testing on a 1:80 scale model of a similar 112 m Incat Tasmania high speed catamaran. The mass of their scale model was 5.86 kg with a design water line at 0.055 m above the base. In their paper, no reference was made to the effect of the boundary layer profile shape. For comparative purposes, the wind velocity for this study was set at 14.25 m/s to achieve Reynolds number similarity with their tests at 3.8 m/s. The vessel angle is varied from 0° to 180° at 15° intervals. This comparison is extensively described in Amani, (2019). The focus of this paper is to study the manoeuvrability of a large catamaran at low speed and not the design requirements to withstand severe sea loading defined by international maritime organisation (IMO). While severe wind loading recommendations are available (IMO, 2005) the wind velocity for this study was set to achieve Reynolds number similarity with the tests of Oura & Ikeda, (2007) for purpose of comparison.

2.1 SCALE MODEL

The scale model of the ship was made using a 3D resin printer. The 1:300 scaled model was bonded to a disk with the Cartesian coordinate system shown in Figure 4. The disk was inserted into a recess inside the fixed platform and then connected by a strut to a load cell which is mounted below and outside of the wind tunnel test area. The top surface of the disk was level with the top surface of the platform and the disk was rotated from 0° to 180°. The platform was bolted to the side walls of the wind tunnel test area and creates two separate regions inside the test area.

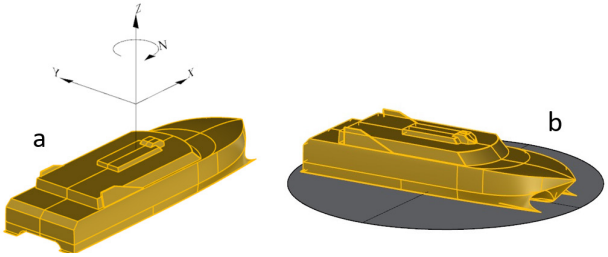

Figure 4. a) Definition of ship coordinate system. The ship coordinate system is not necessarily always the same as the experimental domain or the load cell coordinate system. b)The scaled model was bonded to the rotating disk

The leading and trailing edge of the platform were designed to minimise flow separation and disturbance in the test area by using a NACA 0010 profile. The complete assembly showing the model positioned inside the wind tunnel set up is shown in Figure 5. The model testing conditions were appropriately measured and controlled to maintain similitude (Lutz, 1997). Air temperature, density and humidity inside the wind tunnel were measured to enable accurate determination air density, viscosity and dimensionless parameters.

2.2 SOLID BLOCKAGE RATIO

The calculated blockage ratio based on the model frontal area and the wind tunnel cross section above the platform was 5.8%. Rae & Pope, (1984) recommend that the maximum solid blockage ratio in wind tunnel testing should be less than 7.5%, which is greater than the blockage ratio used for wind tunnel testing. Therefore, no correction factor was applied.

2.3 WIND TUNNEL EXPERIMENT

Prior to starting the wind tunnel experiment and before mounting the model on the platform, the velocity profile at different locations on the platform was measured in order to determine the longitudinal position where the velocity boundary layer profile most closely matched the atmospheric boundary layer. The approach of locating

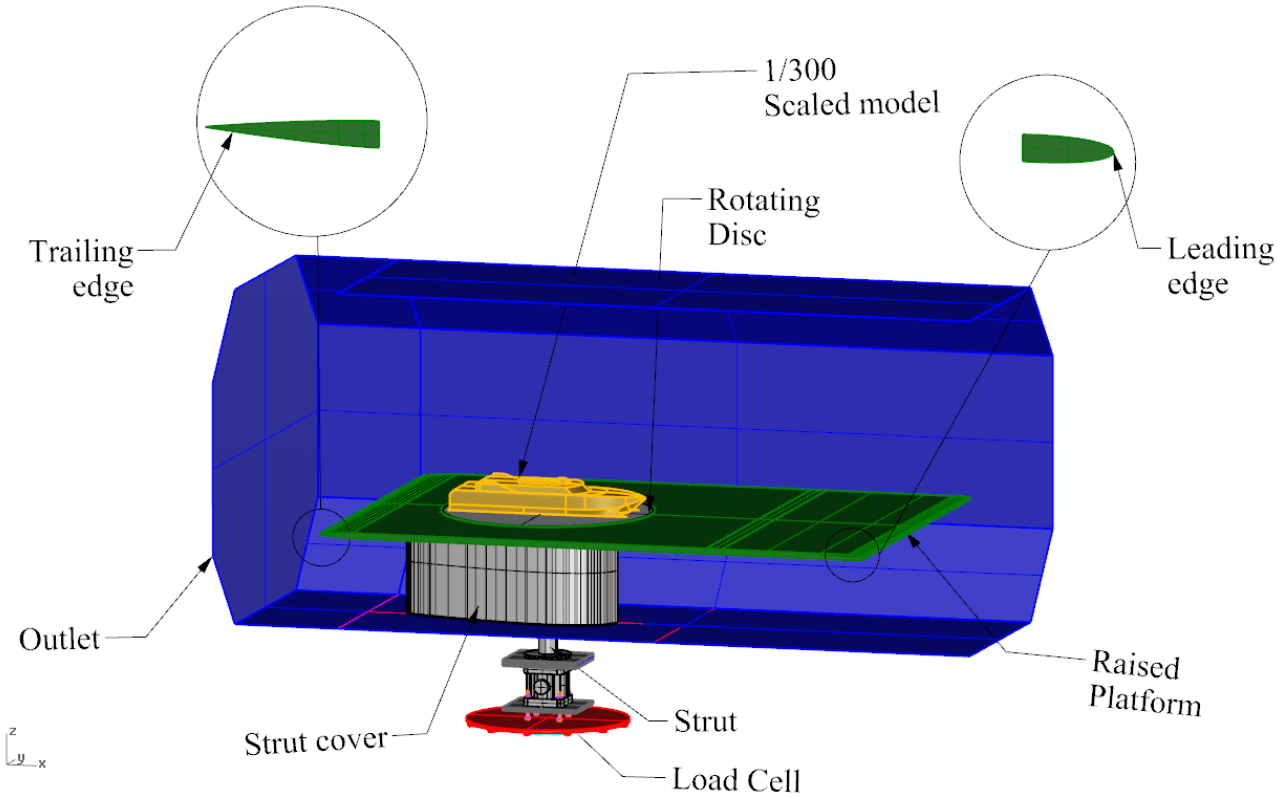

Figure 5. The isometric view of the wind tunnel assembly. Sections of the leading and trailing edge are shown at a larger scale to assist visualisation. The figure also shows how the strut cover is fitted between the floor of the wind tunnel and the underside of the raised platform to protect the strut from any wind loads.

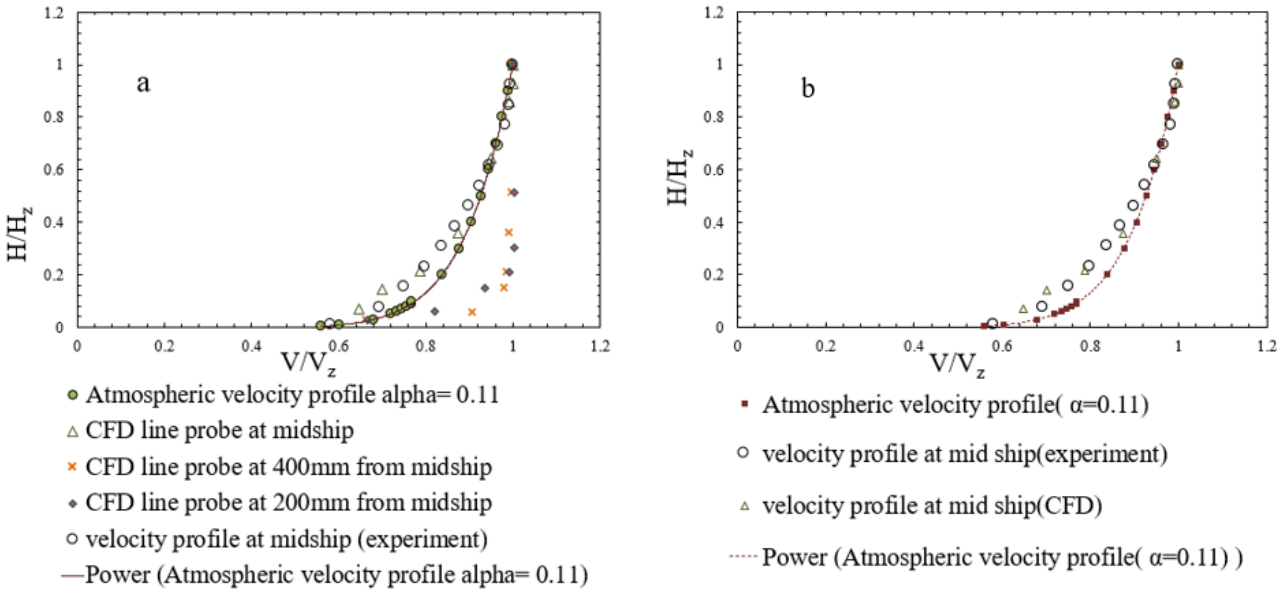

Figure 6. a) Velocity profiles in the wind tunnel (experiment and CFD);
b) Comparison of the velocity profile in wind tunnel and CFD model

the test model in the wind tunnel in such a position that the velocity profile is close to the natural velocity profile in the ocean was previously used by Andersen, (2012) and Janssen *et al.,* (2017). The velocity profile was measured by a pitot tube while the average air speed was maintained at 14.25 m/s. Hot wire probes (DT 8880 and TSI Veloci Calcs Plus) were used for additional velocity readings. Each set of readings were non-dimensionalised and compared against the atmospheric velocity profile. It was found that the non-dimensional velocity profile at 700 mm downstream from the leading edge of the platform compared favourably with the atmospheric boundary layer

on the ocean (with α = 0.11). V_z is the reference value for the wind speed on the ocean which is usually at a 10 m height from the water surface (Larsson *et al.,* 2003). At 1:300 scale, the 10 m height corresponds to 33.3 mm (H_z) in the wind tunnel experiment. Similar analysis was performed using CFD. Results from the experiment and the CFD results at mid ship were very close to the atmospheric boundary layer profile. After installation of the model, the boundary layer was again measured in-line with the midship position to confirm the model setup.

Figure 7 shows the scale model of the ship mounted on the rotating disk inside the wind tunnel. The load cell is located below the wind tunnel and is mounted on a rotary table. The ship's coordinate axes are aligned with the wind tunnel axes but perpendicular to the load cell.

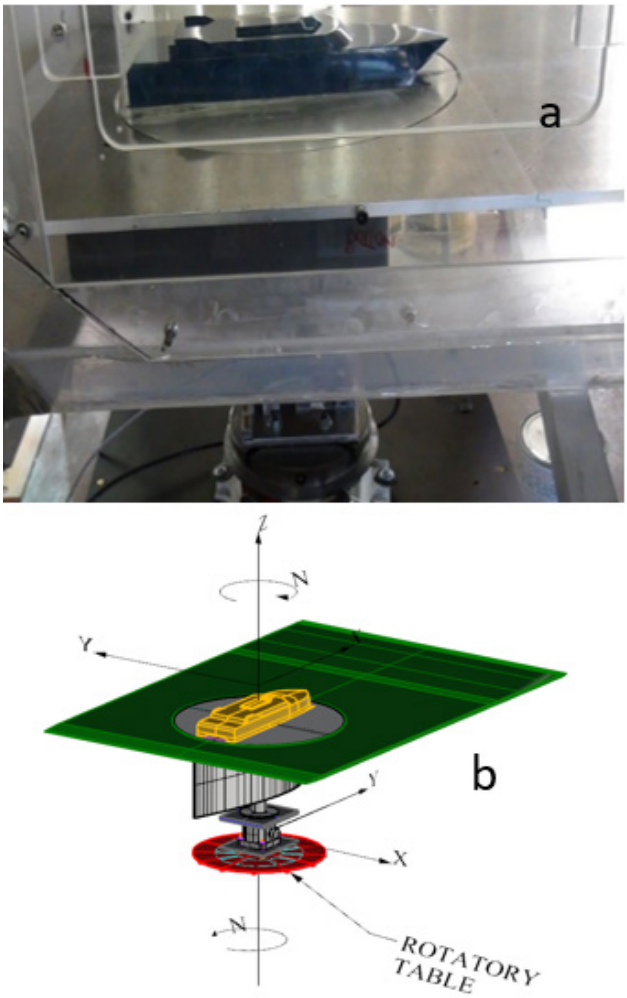

Figure 7. a) 1:300 scale model of the ship glued onto the top surface of the rotating disc. The ship's model is set at zero degrees when the wind is directly blowing into the bow. b) The coordinate system of the load cells.

The positive x axis of the wind tunnel test area is from its outlet to the inlet. The zero-degree heading was determined by confirming a zero-side force was measured while the wind tunnel was running. Longitudinal and transverse forces coefficients and the moment coefficient were defined as:

$$C_x = \frac{F_x}{\frac{1}{2}\rho_a S_F U_W^2} \tag{2}$$

$$C_y = \frac{F_y}{\frac{1}{2}\rho_a S_L U_W^2} \tag{3}$$

$$C_N = \frac{M_Z}{\frac{1}{2}\rho_a S_L L U_W^2} \tag{4}$$

3. CFD SIMULATIONS

A CFD model was created to replicate the wind tunnel experimental cases for all angles tested. The aim of this was to validate the results from CFD against the results from the wind tunnel test. The CFD domain size was set to match the wind tunnel model. All CFD analyses were performed in steady state. RANS CFD simulations were conducted using Star-CCM+ with geometry matching the proposed experimental set up as closely as possible. This was done with the aim to enable validation of the numerical simulation such that the simulation could be used to provide additional results at higher speeds and ship sizes. A sensitivity analysis was conducted using two turbulence models, Realisable $k - \varepsilon$ and *SST* $K - \omega$. The inlet flow is uniform and initial setting for turbulence intensity at inlet is 0.01. Results showed negligible difference between the magnitude of the force coefficients for the two models. It is widely acknowledged that Realisable $k - \varepsilon$ performs better than many other 2-equation models for separated flows, swirling and rotating flows with two layer "all y+" wall treatment which allows for a combination of coarse and fine meshes as boundary layers develop. The *SST* $K - \omega$ does not need two-layer treatment (Tu *et al.* 2013). RANS based CFD simulations are well accepted for determination of wind load coefficients on structures. Pena and Huang, (2021) notes that model scale investigations using RANS have reached a certain maturity and confidence. Many comparisons between RANS-CFD and experimental model tests show good agreement for open-water resistance, propulsion, seakeeping and manoeuvring simulations.

A hex-dominant mesh with 8 prism layers was used. Local refinement was undertaken to capture the complete behaviour of the fluid flow around the model. For

Table 2: Typical grid setting in CFD domain for all CFD analyses.

Type of mesh	Hex-dominant
Number of cells	13465353
Prism layer thickness	0.00125 m
Number of prism layers	8
Prism layer stretching	1.5

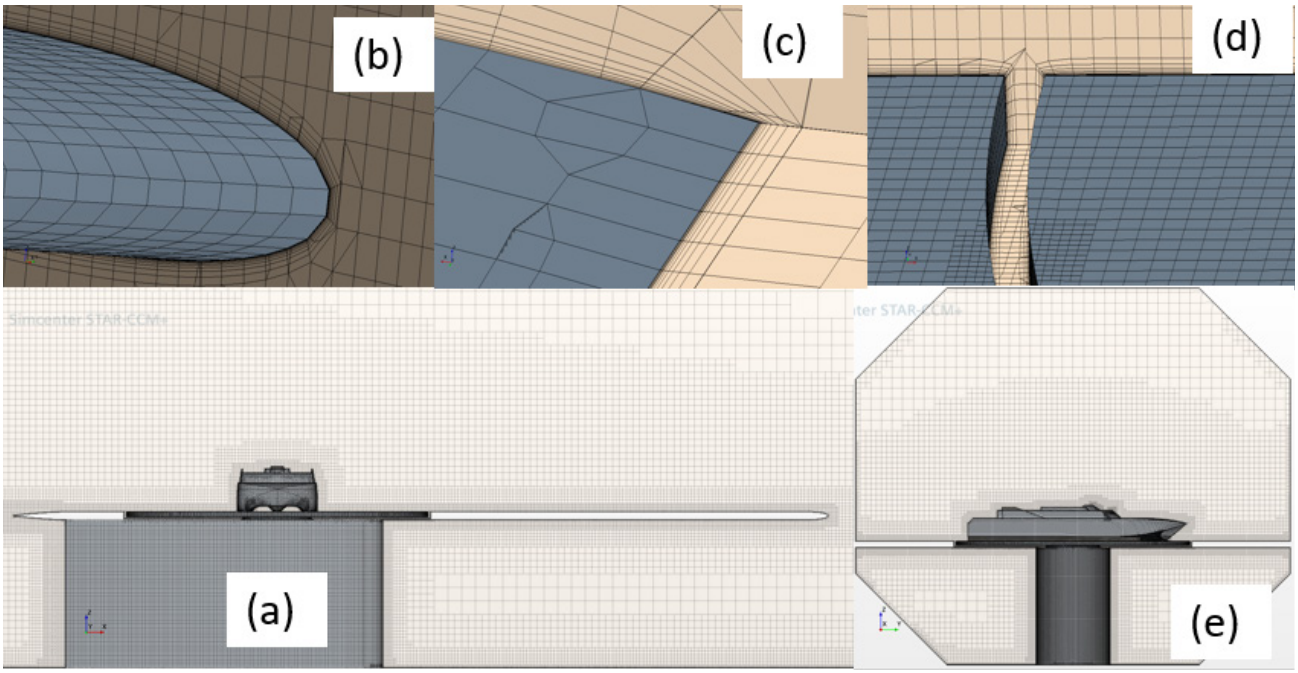

Figure 8: CFD mesh prism layer detail. The model is at a 90° heading to the wind.
a) Front elevation. b) The leading edge of the platform. c) The trailing edge of the platform.
d) The gap between the rotating disk and the platform front elevation. e) Side elevation.

verification, further mesh refinements in both prism layer and core area were conducted. Table 2 details the mesh settings of the CFD model. The general mesh and physics settings for this model are typical for all other angles, though the number of cells varies slightly between each model. Figure 8 shows the general mesh refinement in the CFD domain.

4. RESULTS

Figure 9 shows the CFD model results at a 45° heading. The streamline plot demonstrates the expected recirculation zone behind the model. A low-pressure zone inside the ship's tunnel (space between the ship's demi hulls), behind the ship, forces the air velocity to increase in those regions,

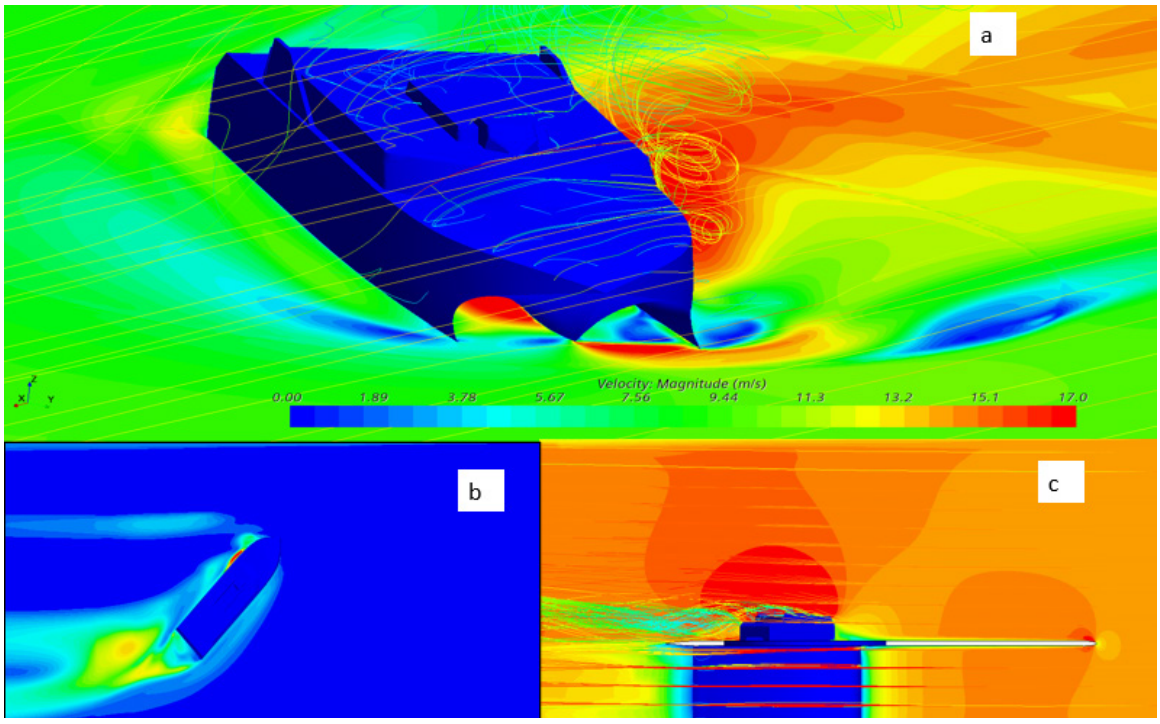

Figure 9: CFD velocity contours (wind speed of 14.25 m/s). Wind angle of attack is 45°. A) Isometric with wind streamline. B) Turbulent Kinetic energy (TKE) contour. C) Elevation with streamline. Section at midship.

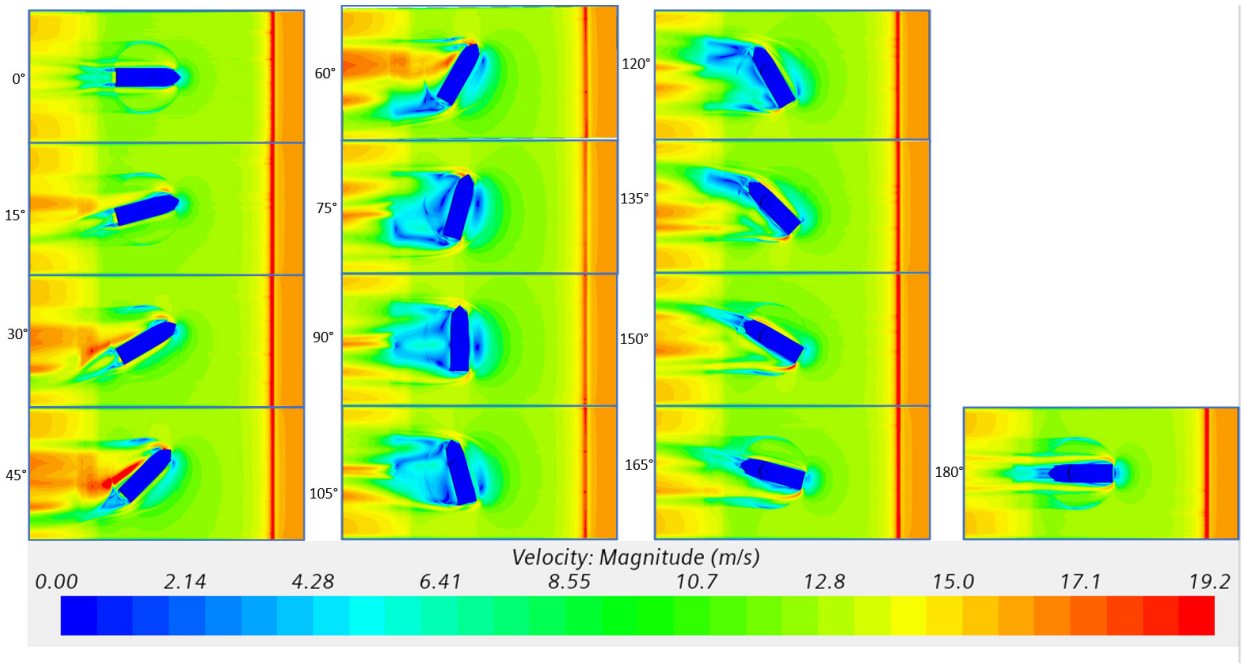

Figure 10: Velocity contours plots (wind speed of 14.25 m/s). The wind angle of attack is from zero to 180°. Velocity contour plane is at (0,0,0.204)m above the floor of the wind tunnel.

resulting in an increase of the lift force on the ship. The behaviour of the wind in the air wake of the ship (bluff body) has a very high level of turbulence coupled with large gradients of wind velocity. Plots of velocity magnitude and turbulent kinetic energy are also shown.

Figure 10 shows contours of air velocity magnitude around the ship for each of the headings analysed. The results from CFD analysis shows an increase in the velocity magnitude behind the ship when the wind angle of attack changes from 15° to 60° heading and is maximum when the wind angle of attack is at 45°. This behaviour can be explained as a result of the ship acting as an aerofoil and producing a transverse lift force. Post-processing and interrogating the CFD results provide high level detail of the complex flow around a vessel. Those results can assist in implementing ways to enhance the ship performance in way of reducing the forces in relative winds from all direction. (i.e., reshaping the hull and superstructure of the ship to be more aerodynamic and reducing sharp edges to minimise, flow separation and recirculation zones)

4.1 VERIFICATION AND VALIDATION

In the current arrangement of the wind tunnel, the ship and the rotating disk are a single assembly. Therefore, the load cell measures the total shear and pressure drag on both the model and the rotating disc, ($f_{(ship)} + f_{(disc)}$) as both these parts are experiencing wind loading. During the test and each time, the ship was rotated, the size and the intensity of the recirculation zone behind the scale model changes the effects of the magnitude of the force and moment on the rotating disc. Therefore, for validation of the CFD model, the measured forces and moments on both the ship model and the rotating disk were measured from CFD analysis and compared with similar measured forces given by the load cell during the wind tunnel test.

4.1(a) Verification

Verification was performed with consideration to iterative U_i, grid U_G, prism layer U_P and physical studies (difference between turbulence models) U_{PH}.

$$U_{SN}^2 = U_i^2 + U_G^2 + U_P^2 + U_{PH}^2. \quad (3)$$

All CFD simulations were performed in steady state and all residuals had monotonic convergence. According to Stern et al., (2006), when verification studies show oscillatory behaviour (between the solutions on each grid) the uncertainty value of U_x can be calculated from; $U_x = \frac{1}{2}(S_u - S_L)$ when S_u *and* S_L are the maximum and minimum of the last iteration oscillation, where x denotes the uncertainty type of interest. Four grid sizes using a refinement ratio of $\sqrt{2}$ were used. The results from CFD and EFD are shown in Table 3:

Table 3: Numerical results from four meshes (wind direction = 45°, Re = 3.2×10^5)

	Base size	C_x	C_y	C_N
CFD Grid 1	0.035	0.147	0.895	0.068
CFD Grid 2	0.05	0.139	0.89	0.071
CFD Grid 3	0.06	0.15	0.909	0.064
CFD Grid 4	0.07	0.136	0.912	0.067
EFD	–	0.157	0.815	0.070

In each analysis, values for U_i, U_G, U_P, & U_{PH} were calculated. The results are summarised in Table 4.

Table 4: summary of uncertainty analysis for grid, iteration, etc.

	U_i%	U_G%	U_p%	U_{pH}%
C_x	0.05	4.83	0.14	0.34
C_y	0.02	1.23	0.12	0.11
C_N	0.00	4.74	0.51	3.28

Finally, the total uncertainty of the numerical analysis was calculated by using equation (2). The total CFD uncertainty (USN) calculated as UC_x = 4.84% UC_y = 1.24% and UC_N = 5.79%

4.1(b) Experimental Uncertainty

The wind tunnel test data were used as a benchmark data for the validation of the CFD results. Therefore, the wind tunnel data was converted to non-dimensional form. The uncertainty due to measurement of density, velocity, area and length were combined to calculate the total uncertainty values for C_x, C_y and C_N using the propagation of uncertainty method (Figliola & Beasley, 2019). The total EFD uncertainty (*UD*) calculated as: UC_x = 8.44%, UC_y = 8.92% and UC_N = 7.4%.

4.2 VALIDATION

The comparison error E is defined by the difference between experimental data D and simulation S values. $E = D - S = \delta_D - (\delta_{SM} - \delta_{SN})$ where δ_d is experimental error, δ_{SM} is modelling error and δ_{SN} is the total numerical error. To determine if the validation has been achieved, the comparison error is compared to validation uncertainty U_V. If $|E| < U_V$, the combination of all the errors in D and S is smaller than U_V and validation is achieved (Stern *et al.* 2006). U_V is calculated as:

$$U_V^2 = U_D^2 + U_{SN}^2 \quad (4)$$

U_D is experimental and U_{SN} is numerical uncertainty. As it is shown in the following tables the value of E is less than U_V and validation is achieved at the uncertainty U_V.

Table 5: Validation of C_x, C_y And C_N.

	E%	*UV*%	*USN*%	*UD*%
C_x	7.64%	9.73%	4.84%	8.44%
C_y	8.99%	9.00%	1.24%	8.92%
C_N	2.42%	9.36%	5.8%	7.4%

4.2(a) Reynolds Number Effects

To investigate the effect of Reynolds number, analysis was performed in range of wind speeds and scales. The summary is shown in the Table 6

Table 6: Reynolds Number for various scale and wind velocity

	U (m/s)	L (m)	Re
Oura & Ikeda, (2007)	3.8	1.32	$3.20 \cdot 10^5$
EFD (low U)	14.25	0.352	$3.20 \cdot 10^5$
EFD (Mid U)	20	0.352	$4.49 \cdot 10^5$
EFD (High U)	28.5	0.352	$6.40 \cdot 10^5$
Full Scale	14.25	105.6	$9.60 \cdot 10^7$

Full scale results were obtained by scaling the 1:300 scale model results and re-meshing the computational domain. Mesh refinement at leading edges and the recirculation zone. The speed of 14.25 m/s (average speed of a 112m catamaran) was used for full scale analysis to investigate the effect of large Reynolds number.

There are significant differences in results between Ikeda and the current CFD and EFD as shown in Figure 11. The longitudinal force coefficient (C_x) in quarter and following winds is showing a different trend. The differences between the results could be explained by differences in the boundary layer profiles, but this cannot be verified profile data was not reported by Oura & Ikeda, (2007). Also, no reference was made to the use of a blockage correction factor. The difference between model scale and full-scale data indicates that further work at full scale is warranted.

4.3 EFFECT OF DISK IN WIND TUNNEL TESTS

As explained in Section 4.1, that for validation the results of wind loading on both model and disk was compared between EFD and CFD. Next CFD analysis was used to extract the wind forces and moments on scale model only. These results are shown in Table 7 and can be used in the station keeping study of 112m high-speed wave piercing catamaran.

For comparison, the simulated and measured coefficients for the combined ship and disk along with the computed coefficients for the ship only are presented in Figure 12. As is shown all results are in a close agreement. Close agreement in force and moment values validates the results from the CFD simulations.

The disk is exposed to the wind forces due to skin friction and pressure. For comparative purposes both the CFD models with and without the disk are included. The graph of C_x shows an increased force value including the disk for a headwind (0°), and this difference is reversed for a

tailwind (180°). A similar effect of wind loading on the disk is observed in the graph of C_y where increased skin friction acting on the disk at 90° contributes to an increased force coefficient as the shear is aligned with the y-axis.

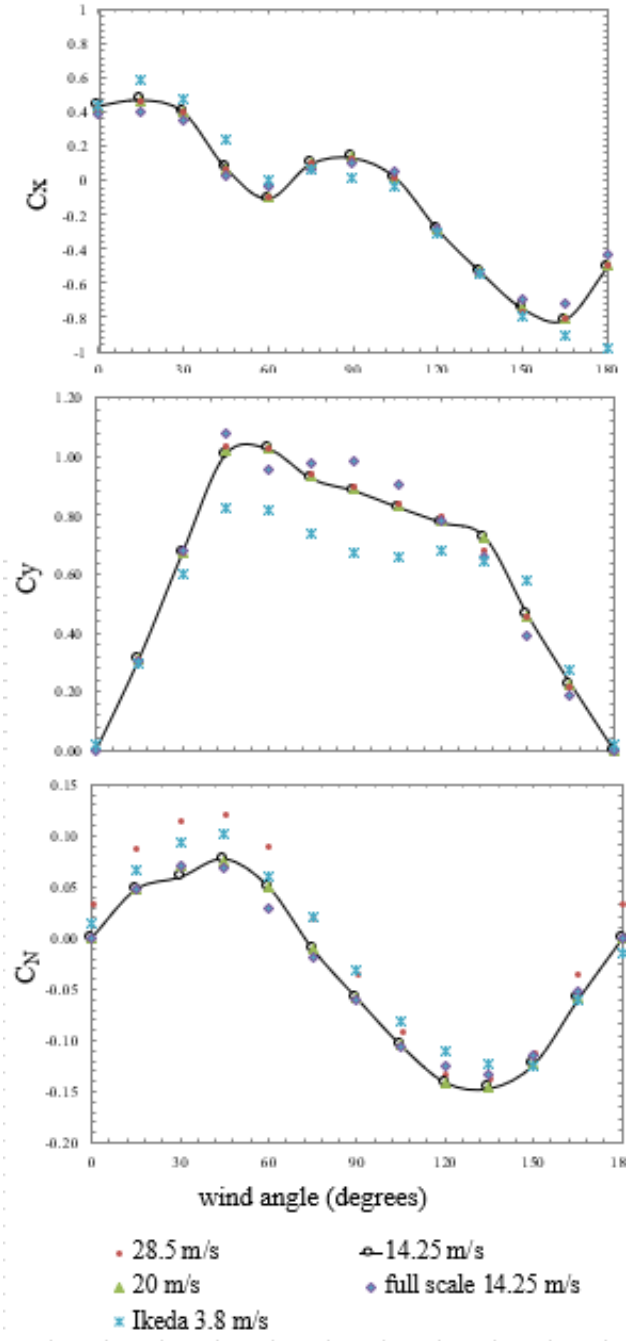

Figure 11: Comparison of the wind force coefficients at different wind velocities with full scale Amani, (2019) and results (, and) Oura & Ikeda, (2007).

5. CONCLUSIONS

The station keeping study of large high-speed wave piercing catamarans determines if their propulsion systems are sufficient for manoeuvring the vessel or if additional equipment (for example, thrusters) is required to be installed on the ships. The ability to travel on the intended course with more control and manoeuvrability, especially at lower speed determines the required specification for this machinery. Several conclusions from outcomes of experimental and numerical studies of wind forces acting on a 1:300 scale model of Incat 112 m high speed wave piercing catamaran may be made. In order to minimise the effect of the side walls on the flow field, the model was positioned in the widest part of the wind tunnel by raising the model from the floor of the wind tunnel and mounting it on a new platform. This also allowed control over the boundary layer velocity profile, which was made similar to the natural velocity profile above the ocean's surface. In doing so, it was not necessary to apply correction factors as in previous work (Andersen, 2012 and Janssen *et al.,* 2017). It is also shown that the effect of the atmospheric boundary layer in the final results could be significant. This has been carefully documented in this study. Uncertainty analysis in CFD was carried out with four sets of hex-dominant grids. The uncertainty of the CFD results is less than 6% and validation was achieved. This study shows that CFD can be used as a reliable tool to predict the aerodynamic performance of high-speed wave-piercing catamarans, and also as a design tool to improve experimental design and assess experimental effects such as blockage ratio. It is shown that the calculated wind force and moment coefficients from experimental tests and CFD analysis in scale models are accurate and can be used in further station keeping studies of that particular ship. The ability to post-process and interrogate the CFD results provides high level detail of complex flow on vessel, over a range of scales.

Table 7: non-dimensional force and moment coefficients on scale model only.

	Results from CFD 1:300 scale		
Θ (deg.)	C_x	C_y	C_N
0	0.438	0	0
15	0.476	0.311	0.047
30	0.407	0.669	0.07
45	0.079	1.006	0.077
60	–0.104	1.024	0.05
75	0.099	0.923	–0.011
90	0.136	0.881	–0.059
105	0.021	0.826	–0.105
120	–0.286	0.774	–0.141
135	–0.534	0.682	–0.146
150	–0.75	0.457	–0.123
165	–0.667	0.206	–0.059
180	–0.5	0	0

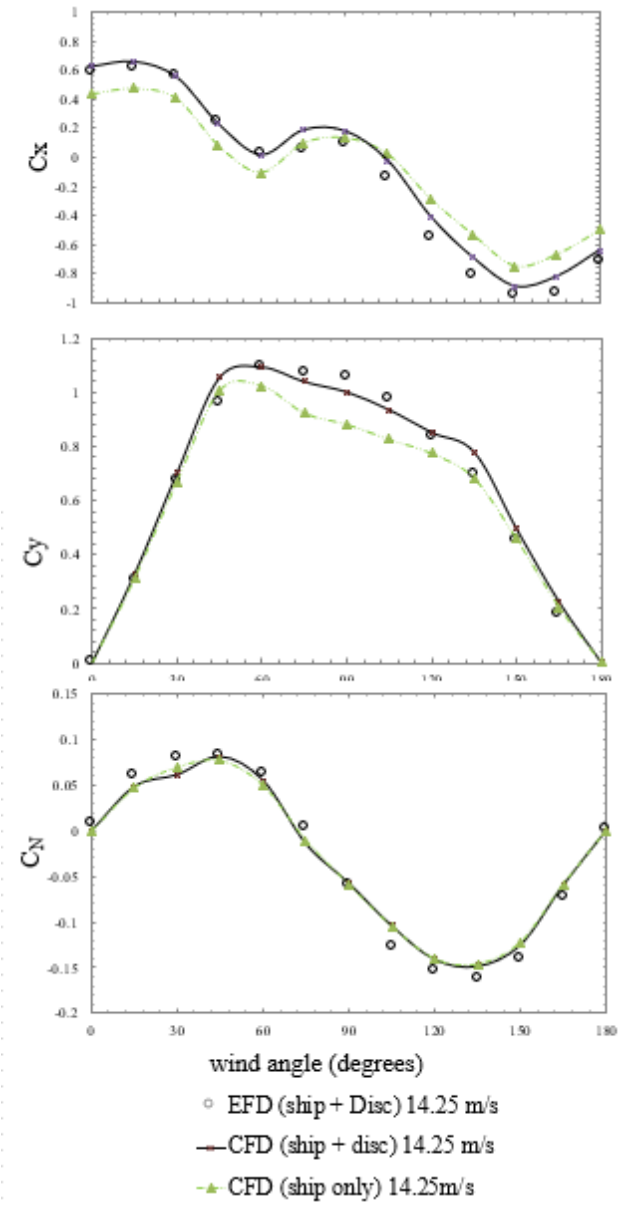

Figure 12: Non-dimensional force coefficients for the wind tunnel experiment and the CFD analysis on both the ship and the rotating disc, and for the ship only.

6. RECOMMENDATIONS

Waves and currents could play a much more important role on manoeuvring of a vessel. Wind generated waves will also affect manoeuvrability. The coupled effects of waves, currents and wind loading must be included for a more realistic analysis. This will be the topic for future work. However, the focus of this paper is only on effect of the wind loading on performance of a high-speed catamaran. It is recommended that future research considers both air and water in both experimental and CFD studies which includes the effect of current and waves in calculating the total forces acting on a ship since the water induced loads can be dominating in exposed ports or areas with tidal/river currents. Further work on full scale analysis is recommended. It is also recommended that this study is continued to find effective methods to reduce the effect of strong winds on larger high-speed catamarans, especially when they are travelling at low speed in harbour. Higher fidelity CFD models such as DES were not deemed necessary for this study, but will be considered for future work in full scale analysis and when wave and current are coupled in analysis.

7. AKNOWLEDGEMENTS

The authors would like to thank Dr Nagi Abdussamie and Dr Zhi Leong of AMC for providing general feedback and discussion. The authors also would like to thank the staff members of the University of Tasmania workshop for fabrication and assembly of the wind tunnel test area and load cell for the wind tunnel experiment. Special thanks to Calverly Gerard for the calibration of the load cell and data acquisition program.

8. REFERENCES

1. AAGE, C, HVID, SL, HUGHES, PH and LEER-ANDERSEN, M (1997). *Wind loads on ships and offshore structures estimated by CFD*, in JH Vughts (ed.), 8th International Conference on the Behaviour of Offshore Structures, BOSS'97, Elsevier Science Ltd., Pergamon, Delft, The Netherlands, vol. 2.
2. AMANI, S (2019). *Numerical and experimental analysis of the wind forces acting on a high speed catamaran*, Masters of Philosophy (Maritime Engineering) thesis, University of Tasmania (AMC).
3. ANDERSEN, IMV (2012). *Wind-tunnel investigation of wind loads on a post-panamax container ship as a function of the container configuration on deck*, in International Marine Design Conference, 11-14 June, Glasgow UK, 2012.
4. COLEMAN, HW and STEELE, WG (2018). *Experimentation, validation, and uncertainty analysis for engineers*, 4th Ed., John Wiley & Sons, Hoboken, New Jersey.
5. FIGLIOLA, RS and BEASLEY, DE (2019). *Theory and design for mechanical measurements*, 7th Ed., John Wiley & Sons, Hoboken, New Jersey.
6. FORMELA, K (2018). *Comparison of the Calculated Wind Loads to the Power Generated by the Main Propulsion and Thrusters of the Ship with the Results of Simulation Tests*', TransNav: International Journal on Marine Navigation and Safety of Sea Transportation, vol. 12.
7. FORREST, J and OWEN, I (2010). *An investigation of ship airwakes using Detached-Eddy Simulation*, Computers & Fluids, vol. 39 (4): 656-673.

8. FRANK, J, and HELLSTEN, A, and SCHLÜNZEN, H and CARISSIMO, B (2007). *Best practice guideline for the CFD simulation of flows in the urban environment*. COST action 732', Quality Assurance and Improvement of Meteorological Models. University of Hamburg, Meteorological Institute, Center of Marine and Atmospheric Sciences, Meteorological Inst., Brussels, Belgium.
9. FUJIWARA, T, and UENO, M and NIMURA, T (1998). *Estimation of wind forces and moments acting on ships*, Journal-Society of Naval Architects of Japan, vol. 183, pp. 77-90.
10. HSU, S, and MEINDL, EA and GILHOUSEN, DB (1994). *Determining the power-law wind-profile exponent under near-neutral stability conditions at sea*, Journal of Applied Meteorology, vol. 33, no. 6, pp. 757-765.
11. IMO, RA (2005). *Recommendation on a Severe Wind and Rolling Criterion (Weather Criterion) for the Intact Stability of Passenger and Cargo Ships of 24 metres in length and over*, Technical Report IMO A. 562 (14), International Maritme Organization, UK
12. JANSSEN, WD and BLOCKEN, B and VAN WIJHE, HJ (2017), *CFD simulations of wind loads on a container ship: Validation and impact of geometrical simplifications*, Journal of Wind Engineering and Industrial Aerodynamics, vol. 166, pp. 106-116.
13. LARSSON, L and RAVEN, H (2010). *Ship resistance and flow*, Society of Naval Architects and Marine Engineers, First. Ed., Jersey City, New Jersey.
14. LARSSON, L, and STERN, F and BERTRAM, V (2003). *Benchmarking of computational fluid dynamics for ship flows: the Gothenburg 2000 workshop*, Journal of Ship Research, vol. 47, no. 1, pp. 63-81.
15. LUBITZ, W and WHITE, B (2004), *Atmospheric boundary layer wind tunnel applications in wind turbine siting*, Proceedings of World Wind Energy Conference, 2004. Beijing, China, Oct. 31 – Nov. 4. 2004b
16. LUTZ, T (1997). *The effect of the boundary layer present in wind tunnels on the aerodynamic drag of a model truck*, MSc Thesis, Department of Mechanical Engineering, University of Cape Town.
17. MAJIDIAN, H and AZARSINA, F (2018), *Aerodynamic Simulation of A Containership to Evaluate Cargo Configuration Effect on Frontal Wind Loads*, China Ocean Engineering, vol. 32, no. 2, pp. 196-205.
18. OURA, T and IKEDA, Y (2007). *Maneuverability of a Wavepiercing High-Speed Catamaran at Low Speed in Strong Wind*, paper presented to 2nd International Conference on Marine Research and Transportation, June 28th to June 30th 2007, Ischia, Naples, Italy.
19. PENA, B and HUANG, L (2021). *A review on the turbulence modelling strategy for ship hydrodynamic simulations*, Ocean Engineering, vol. 241, p. 110082.
20. POLSKY, S (2002). *A computational study of unsteady ship airwake*, in 40th AIAA Aerospace Sciences Meeting & Exhibit, 14-17 Jan, Reno, Nevada, p. 1022.
21. RAE, W and POPE, A (1984). *Low-speed wind tunnel testing, 1984*, 2nd Ed., John Wiley, New York, USA.
22. SADOVNIKOV, D (2009). *Station keeping of high speed ferries*, in International Conference on Innovation in High Speed Marine Vessels, Fremantle, Australia, pp. 39-48.
23. STERN, F, and WILSON, R and SHAO, J (2006). *Quantitative V&V of CFD simulations and certification of CFD codes*, International journal for numerical methods in fluids, vol. 50, no. 11, pp. 1335-1355.
24. STERN, F, and WILSON, RV, and COLEMAN, HW and PATERSON, EG (1999). *Verification and validation of CFD simulations*, Iowa Inst Of Hydraulic Research Iowa City. Report No. 407.
25. TASUMI, H and IKEDA, Y (1999). *Maneuverability of a high-speed catamaran running at low speed in strong wind*, The 4th Japan-Korean Joint Workshop On Ship And Marine Hydrodynamics, 12-13 July, Fukuoka, Japan
26. TOMINAGA, Y, and MOCHIDA, A, and YOSHIE, R, and KATAOKA, H, and NOZU, T, YOSHIKAWA, M and SHIRASAWA, T (2008). AIJ *guidelines for practical applications of CFD to pedestrian wind environment around buildings*, Journal of Wind Engineering and Industrial Aerodynamics, vol. 96, no. 10-11, pp. 1749-1761.
27. TU, J, and YEOH, GH and LIU, C (2013). *Computational fluid dynamics: a practical approach*, 2nd edn, Butterworth-Heinemann, Waltham, MA.
28. VOGT, JW, and BOVIO, M and MALLOL, B (2017). *Validation of Wind Loads on a Slender Vessel using CFD*, 20th Numerical Towing Tank Symposium (NuTTS), 1-3 October, Wageningen, The Netherlands.
29. WNĘK, A, and PAÇO, A, and ZHOU, X and SOARES, CG (2010). *Numerical and experimental analysis of the wind forces acting on LNG carrier*, in *Fifth European Conference on Computational Fluid Dynamics*, 14-17 June, Lisbon, Portugal.

